

Soft X-ray emissions of Si IX in Procyon

Guiyun Liang^a and Gang Zhao^{a *}

^a*National Astronomical Observatories, Chinese Academy of Sciences, Beijing
100012, P. R. China*

Abstract

An analysis of $n = 3 \rightarrow 2$ transition lines of carbon-like silicon reveals that some ratios of line intensities are sensitive to the electron density. The ratio between two group of $3d \rightarrow 2p$ transition lines at 55.246 Å and 55.346 Å is a good n_e -diagnostic technique, due to its insensitivity to the electron temperature. Using this property, a lower limit of the density of $0.6 \times 10^8 \text{ cm}^{-3}$ is derived for Procyon, which is consistent with that constrained by C V and Si X emissions. Significant discrepancies in ratios of $3s \rightarrow 2p$ lines to $3d \rightarrow 2p$ lines between theoretical predictions and observed values, are found, by the spectral analysis of Procyon observed with the *Chandra* High Resolution Transmission Grating spectra. The difference exceeding a factor of 3, cannot be explained by the uncertainty of atomic data. The opacity effect is also not a choice as reported by Ness and co-workers. For the $3s \rightarrow 2p$ line at 61.611 Å, present work indicates that the large discrepancy may be due to the contamination from a S VIII line at 61.645 Å. For the lines at 61.702 and 61.846 Å, we suggest that the discrepancies may be attributed to contaminations of unknown lines.

PACS: 95.20.Jg; 97.10.Ex; 95.85.Nv

Key words: stars: late-type; stars: coronae; X-rays : stars

* Corresponding author: Gang Zhao

Email address: gzhao@bao.ac.cn (Gang Zhao).

1 Introduction

Since the launch of the new generation X-ray observatories, *Chandra* and *XMM-Newton*, X-ray spectra with unprecedented spectral resolution and high statistical quality can be obtained for astrophysical objects. The High Energy Transmission Grating Spectrometer (HETGS) and Low Energy Transmission Grating Spectrometer (LETGS) on *Chandra* can provide resolving power of $\lambda/\Delta\lambda \sim 100-1000$ and ≥ 1000 in wavelength ranges of 1.5-30Å and 50-160Å, respectively. The effective areas can be as large as 200 cm² in some energy regions. Using these high-quality spectra, physical conditions of stellar coronae such as electron density, thermal structure, and element abundances, can be derived. Such information further helps to constrain models of the coronal heating and structuring. In the past, the information about the spatial distribution of coronal plasma was inferred by indirect means such as modelling of eclipses and rotational modulation (Güdel et al., 1995, 2003; Siarkowski et al., 1996), and such analyses can only be carried out for very special systems with advantageous geometries. Presently, the electron density (n_e) of stellar coronae can be disentangled from the emission measure ($EM = \int n_e^2 dV$), and determined separately using the X-ray spectra with high-resolution for various late-type stars.

The complexes of He-like “triplets” of C, N, O, Ne, Me, and Si, which include the *resonance* ($r: 1s^2\ ^1S_0 - 1s2p\ ^1P_1$), *inter-combination* ($i: 1s^2\ ^1S_0 - 1s2p\ ^3P_{2,1}$), and *forbidden* ($f: 1s^2\ ^1S_0 - 1s2s\ ^3S_1$) lines, are covered by the HETGS and/or LETGS on *Chandra* and Reflection Grating Spectrometer (RGS) on *XMM-Newton*, and are resolvable. Gabriel & Jordan (1969) pointed out the potential diagnostic application of these features for hot plasmas. Recently, Por-

quet & Dubau (2000) recalculated line intensities by accounting for other processes such as dielectronic recombination and radiative recombination. In the HETGS observation of Capella, Canizares et al. (2000) estimated a density range of $0.8\text{-}2 \times 10^{10} \text{ cm}^{-3}$ from O VII, and upper limits near 7×10^{11} and $1 \times 10^{12} \text{ cm}^{-3}$ by Mg XI and Si XIII. Using the LETGS observation of Capella, Brinkman et al. (2000) derived a density of $\sim 2.6 \times 10^9 \text{ cm}^{-3}$ by C V for the lower temperature component of a multi-temperature structure. Later, Ness et al. (2002) and Testa et al. (2004) performed coronal density diagnostics with He-like triplets for other late-type stars with various activities such as Algol, Procyon, α Cen A&B, ϵ Eri, and HR 1099 etc. Using the derived densities, Ness et al. (2004) further estimated the sizes of stellar X-ray coronae, and concluded that the cooler plasma component cannot cover a large fraction of the stellar surface, and there must be spatially separate plasma components at different temperatures. They also argued that the hotter plasma loops fill the space between cooler loops until much of the corona is dominated by the hotter plasma.

The parameter of the electron density is also used to judge the mechanism of the X-ray production. For T Tauri stars, a density of $> 1 \times 10^{12} \text{ cm}^{-3}$ has been obtained from O VII for TW Hya (Stelzer & Schmitt, 2004) and BP Tau (Schmitt et al., 2005), which is higher than typical coronal densities by at least two orders of magnitude. It was assumed that the X-ray emission is produced in the accretion shocks of T Tauri stars, instead of stellar coronae. Additionally, the UV radiative field from the inner layer also plays an important role on the population of levels $^3P_{2,1}$, which directly influences the estimation of n_e . For lighter elements, this effect is more sever (Ness et al., 2001). In the coronal X-ray spectra, in addition of the emissions of H-, He-like ions and Fe L-shell

ions, many lines from highly charged silicon have been observed in the LETGS observations, such as that of Procyon. These emissions may give further insight into the physical conditions of stellar coronae. Recently, we estimated the electron densities and/or temperatures for the cooler components using Si X and Si XI features (Liang et al. 2006a). The emissions from $3d \rightarrow 2p$ and $3s \rightarrow 2p$ transitions of Si IX have also been identified by Raassen et al. (2002) in the LETGS observation of Procyon. In this paper, we investigate the soft X-ray emissions of Si IX in detail.

This paper is organized as followings, observations and measurements of line fluxes are described in Sect.2. Theory model of C-like Si IX is presented in Sect.3. Sect.4 outline the results and discussions, and the conclusion is given in the last section.

2 Observations and line flux measurements

Procyon (F5 IV–V) is a solar-like star at a distance of 3.5pc, with a mass of $1.7M_{\odot}$ and a radius of $2.06R_{\odot}$. So far, three different observations with Low Energy Transmission Grating Spectrometer (LETGS) combined with High Resolution Camera (HRC) are available for this star in the *Chandra* Public Data Archive.¹ The observations are performed on three days, which are summarized in Table 1. We utilized the CIAO3.3 software² and some science threads for the LETGS/HRC observation to reduce the observation data. In order to increase the signal-to-noise ratio (SNR), we co-added these three different observations, resulting in a spectrum with total exposure time of

¹ <http://cxc.harvard.edu/cda/>

² <http://cxc.harvard.edu/ciao/download/>

Table 1

The properties of three different observations of Procyon with LETGS/HRC.

Sequence	Obs_ID	Exposure time	Start time
number		(ks)	
290032	63	70.15	1999.11.6 21:10:29
280411	1461	70.25	1999.11.7 16:58:44
280174	1224	20.93	1999.11.8 12:38:44

159.9ks after times of bad counts were excluded.

Spectral line fluxes were measured using the *Sherpa* software package in the CIAO3.3. Gaussian profile was adopted here, because it can precisely describe the line broadening due to instruments for point-like sources. In the measurements of line fluxes and the determinations of element abundances, the continuum emission plays an important role. It is very difficult to accurately determine the continuum emission in active stars due to its relatively high level. Normal stars, such as Procyon, show very low continuum emission, and do not introduce large uncertainties in the measured line ratios. Here, a constant value of $1.34 \times 10^{-4} \text{phot.s}^{-1} \text{cm}^{-2} \text{\AA}^{-1}$ was adopted to represent the source continuum level, which was determined from the line free region, such as in 51–52Å.

Figs.1 and 2 illustrate the observed spectra with background subtracted in ranges of 54.6–56.0 and 61.5–62.5Å regions, respectively. For lines around 55.0Å, only the positive order spectrum was adopted because of a gap around 54Å in negative order spectrum, while for lines around 62.0Å, the negative

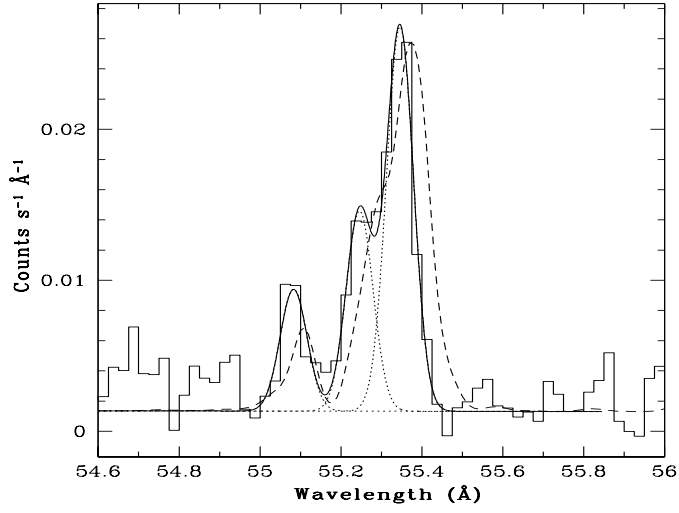


Fig. 1. Observed spectrum of Procyon in wavelength range of 54.6–55.0Å , and best-fit result (solid smooth line) from fitting with three Gaussian profiles (dotted lines) and a constant value. Dashed line represents the synthesized spectrum.

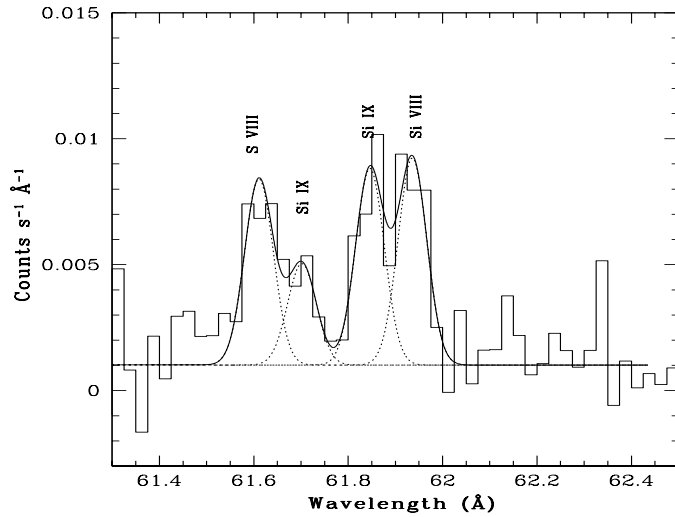


Fig. 2. Observed spectrum of Procyon in wavelength range of 61.5–62.5Å , and best-fit result (solid smooth line) from fitting with four Gaussian profiles (dotted lines) and a constant value.

order spectrum was used due to the gap around 61\AA in the positive order spectrum. Best-fit results (smooth solid lines) are overlaid in the two figures. In the fitting, three and four components with same FWHM were used in the two wavelength ranges, respectively. The line centroid, amplitude of each component, and FWHM are free parameters. Visual inspection and reduced χ^2 (1.1 and 1.3) indicate that the best-fit results are acceptable, which are overlaid in Figs.1-2. Although the resulted line fluxes are slightly over-estimated, they are still within the range of statistical uncertainties (1σ). The line fluxes and identification for features around 55.0 and 62.0\AA are listed in Table 2.

3 Atomic model of Si IX

In our model, the excitations and de-excitations induced by energetic electrons and the subsequent radiative decays among 484 levels belonging to 28 configurations [namely, $(1s)2s^22p^2$, $2s2p^3$, $2p^4$, $2s^22p3l$, $2s2p^23l$, $2s^22p4l$, $2s2p^24l$, $2s^22p5l$ and $2s^22p6l$ ($l = 0, 1, \dots, n - 1$)] have been considered. The optical thin approximation combined with the collision ionization equilibrium can perfectly describe the coronal plasma, and are used extensively in astrophysical modelling, and we adopt this assumption as well. The atomic data, which was calculated using the FAC package (Gu 2003), has been assessed in our previous paper (Liang et al. 2006b). For lower levels, the level populations induced by the collision between the proton and the highly charged Si IX ion, are non-negligible, and we adopt the rates of Rayans et al. (1999) in present analysis. For some weaker transitions, the resonant excitation (RE) process contributes tens of percents to the population. In principle, the excitation rates including resonant effect for all transitions should be included. However,

Table 2

Observed wavelength and flux (in unit of $\times 10^{-4}$ phot. $\text{cm}^{-2}\text{s}^{-1}$) of prominent features in ranges of 54.6–56.0Å and 61.5–62.5Å, and their identification.

Index	λ_{obs} (Å)	Ions	λ_{theo} (Å)	Flux _{obs}	Flux _{theo}		Transition			
1a	55.083	Si IX	55.094	0.68±0.12	0.11	$2s^2 2p 3d$	3P_0	→	$2s^2 2p^2$	3P_1
1b	...	Si IX	55.116	...	0.14	$2s^2 2p 3d$	3P_1	→	$2s^2 2p^2$	3P_1
2a	55.246	Si IX	55.234	1.12±0.14	0.12	$2s^2 2p 3d$	3P_1	→	$2s^2 2p^2$	3P_2
2b	...	Si IX	55.272	...	0.34	$2s^2 2p 3d$	3P_2	→	$2s^2 2p^2$	3P_2
2c	...	Si IX	55.305	...	0.41	$2s^2 2p 3d$	3D_1	→	$2s^2 2p^2$	3P_0
3a	55.346	Si IX	55.356	2.16±0.17	0.76	$2s^2 2p 3d$	3D_2	→	$2s^2 2p^2$	3P_1
3b	...	Si IX	55.383	...	0.15	$2s^2 2p 3d$	3D_1	→	$2s^2 2p^2$	3P_1
3c	...	Si IX	55.401	...	0.70	$2s^2 2p 3d$	3D_2	→	$2s^2 2p^2$	3P_2
4a	61.611	Si IX	61.600	0.75±0.15	0.04	$2s^2 2p 3s$	3P_1	→	$2s^2 2p^2$	3P_0
4b	...	S VIII	61.645	...		$2s^2 2p^4 3s$	$^2D_{5/2}$	→	$2s^2 2p^5$	$^2P_{3/2}$
4c	...	Si IX	61.649	...	0.12	$2s^2 2p 3s$	3P_2	→	$2s^2 2p^2$	3P_2
5	61.702	Si IX	61.696	0.41±0.14	0.03	$2s^2 2p 3s$	3P_1	→	$2s^2 2p^2$	3P_1
6	61.846	Si IX	61.844	0.79±0.16	0.05	$2s^2 2p 3s$	3P_1	→	$2s^2 2p^2$	3P_1
7	61.936	Si VIII	61.914	0.83±0.16		$2s^2 2p^2(^1D) 3d$	$^2F_{7/2}$	→	$2s^2 2p^3$	$^2D_{5/2}$

Notes: The same labels with different lowercase indices (e.g., 3a, 3b and 3c)

indicate blended lines.

for the strong lines we are interested in, the effects of RE appears to be small, and such a model is not necessary. Moreover, the calculation of excitation rates including RE is very difficult for large-scale atomic model. So far, only a few excitation data of Si IX including RE are available, and they are for transitions among lowest levels with $n = 2$ configurations, which were used in our model.

For ions with an open valence shell, such as Si IX, competing between population and de-population for each energy level cause the populations of some levels to be sensitive to the electron density, n_e . Accordingly, some line intensity ratios may also be sensitive. In case of Si IX, we found the ratio between two groups of $3d \rightarrow 2p$ transition lines, the 55.246Å to 55.346Å (the values refer to the resolvable observed wavelengths in Table 2), is sensitive to n_e , as shown in Fig.3. The blending effect from all significant features (refer to Table 2) has been considered in the prediction of the ratio (hereafter R). There are two advantages for n_e -diagnostic using this ratio. One is that the two resolved emissions are the strongest emissions, so they have relatively higher SNR, and the ratio is around unity. The other characteristic is that the ratio is insensitive to the electron temperature T_e as shown in Fig.3. The variation of the ratio is less than 3% when the electron temperature changes 0.2dex. For coronal plasmas ($\log n_e \geq 7.5$), the temperature sensitivity is even weaker.

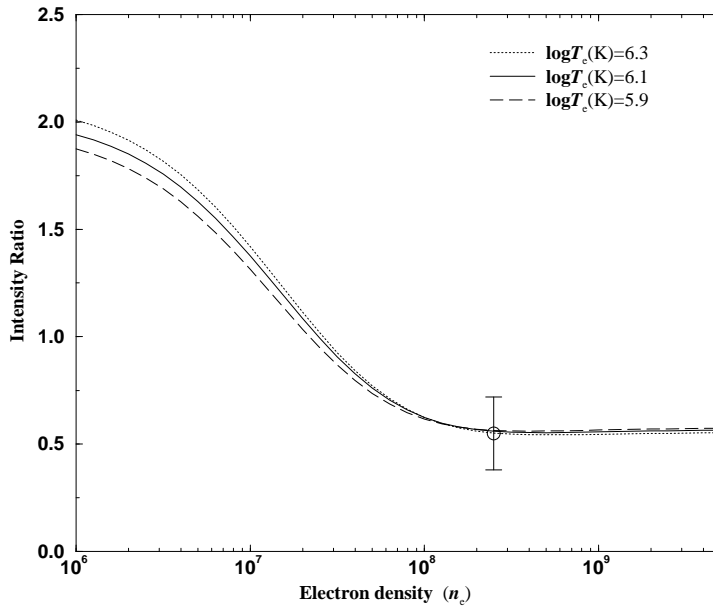


Fig. 3. Predicted line ratio R of two resolvable lines at 55.246 and 55.346\AA , as a function of the electron density n_e at three different logarithmic temperatures (in K) of 5.9 (dash), 6.1 (solid) and 6.3 (dot). The symbol with error bar refers its observed value in Procyon.

4 Results and discussions

4.1 Line identification

In the selected wavelength range, forest-like emissions from highly charged silicon, magnesium, sulfur, calcium and iron are present. Although we disentangled those partially blended emissions through fitting with multi-components, there are several individual lines in each isolated feature. As listed in Table 2, almost all features in this wavelength region, are contaminated. For the line at 55.083\AA , a feature of Mg IX (55.060\AA) may be a source of contribution as reported by Raassen et al. (2002). For the lines at 55.246 and 55.346\AA , several $3d \rightarrow 2p$ transitions of Si IX are identified. Fortunately, no emissions from other charged stages and elements contaminate them. Analysis based on

the line ratio technique for the two groups avoids uncertainties of the element abundance and ionization equilibrium. The blending effect due to $3d \rightarrow 2p$ transitions can be considered in a single-ion model. For the line at 61.611\AA , Raassen et al. (2002) measured a wavelength of 61.578\AA and assigned it to a S VIII line with 61.600\AA . The difference in the measured values of the wavelength might be from the statistic uncertainties and the use of updated calibration files in the present analysis. In the recent experimental work of Lepson et al. (2005), a $3s \rightarrow 2p$ transition line of S VIII is detected at the wavelength of 61.645\AA with a strength of 0.75 relative to that of $3d \rightarrow 2p$ transition line at 52.781\AA , and it is the strongest in the local wavelength range. The obvious detection of $3d \rightarrow 2p$ line in Procyon, indicates that a fraction of the observed flux around 61.611\AA may be attributed to the S VIII line. A search in APEC1.3.1 model (Smith 2001), shows that the emissivity of Si IX line at 61.649\AA is the strongest in this wavelength range. Present model shows a similar result. We also note that the emissivity of Si IX line at 61.696\AA is ~ 0.18 relative to that of 61.649\AA line, so we attribute it to be the possible emission at 61.702\AA , whereas Raassen et al. (2002) measured a wavelength of 61.668\AA and assigned to be a different feature of Si IX at 61.649\AA . The feature at 61.846\AA is presently assigned to be $3s \rightarrow 2p$ transition of Si IX (61.844\AA), because no other prominent transitions are close to this wavelength. The observed line at 61.936\AA is assigned to Si VIII as reported by Raassen et al. (2002).

$3-T_e$ CIE model can describe the observed spectrum satisfactorily as performed by Raassen et al. (2002). One component (with $T_e=1.21\pm 0.07$ MK and $EM = 2.45 \pm 0.27 \times 10^{50} \text{ cm}^{-3}$) of the multi-temperature model is very close to the peak temperature (1.26 MK) of maximum Si IX fraction in the ionization

equilibrium (Mazzotta et al. 1998). In our previous work (Liang et al. 2006a), we derived a density of $2.6 \times 10^8 \text{ cm}^{-3}$ for the cooler plasma of Procyon, using lines of Si X. Using the electron temperature and density, as well as EM and the element abundance estimated by Raassen et al. (2002) for LETGS observation of Procyon, we calculate the theoretical line fluxes as listed in Table 2. The differences between the prediction and observation of line fluxes are primarily from the uncertainty of the element abundance, because their result is from the global fitting of the Procyon spectrum. For $3d \rightarrow 2p$ transitions, good agreements are obtained.

Using Gaussian line profile, we construct a synthesized spectrum of Si IX. The theoretical spectrum normalized to observed line at 55.346 \AA is overlaid on the observed spectrum, as shown by the dashed line in Fig.1. The comparison reveals that the three identified wavelengths around 55.346 \AA appear to have slight more separation in wavelengths, which result in the theoretical spectrum appears broader at this position. This may be from the uncertainty of the atomic data, although the upper levels for these transitions are from NIST³. For line at 55.083 \AA , Raassen et al. (2002) assigned the line flux to be partially from Mg IX emission at 55.050 \AA , while its contribution is very weak as revealed by the present model.

4.2 Estimation of n_e

From the subtracted line fluxes in Procyon, we obtain the observed value (5.2 ± 0.11) for the ratio R . The comparison of the predicted R with the observed value indicates that the electron density is about $> 0.6 \times 10^8 \text{ cm}^{-3}$ in

³ http://physics.nist.gov/cgi-bin/AtData/main_asd

the line emitting region.

In collision ionization equilibrium (Mazzotta et al. 1998), the peak temperature (1.26MK) of Si IX fraction is close to the T_e determined from H- and He-like carbon ions. Therefore, the densities determined by the two different methods should be comparable. However, the radiation effect from Procyon's photosphere has great influence on the estimation of n_e using the triplet ratio of He-like carbon. When this effect has been considered, an upper limit of $< 8.3 \times 10^8 \text{cm}^{-3}$ was obtained (Ness et al. 2002). The combination of the two results definitely gives the density range for the cooler X-ray emitting region. This ratio can also be used to diagnose the n_e for those C-depleted stars, such as Algol.

4.3 Line ratios of $3s \rightarrow 2p$ vs $3d \rightarrow 2p$

Ratios of emission with small oscillator strength f vs emission with large oscillator strength have been used to detect resonant scattering. For example, the ratio of the $3s \rightarrow 2p$ line of Fe XVII at 16.78\AA ($gf=0.01$) to $3d \rightarrow 2p$ line at 15.03\AA ($gf=2.66$) has been used to infer the effects of resonant scattering, because even the most complete model of Doron & Behar (2002) do not agree with the observations, such as the flare observation of AB Doradus (Matranga et al. 2005). Large discrepancies in the predicted and observed ratios for similar lines in Fe XVIII and Fe XIX have also been reported by Desai et al. (2005).

In Procyon, two resolved $3s \rightarrow 2p$ lines have been identified in the work of Raassen et al. (2002). However, the identification is not conclusive due to the uncertainty of atomic data. Here we make a detailed analyses for these possible

$3s \rightarrow 2p$ emissions. For the emission at 61.611\AA , the previous subsection has revealed that a fraction of the observed flux originates from the emission of S VIII line at 61.645\AA . In order to subtract the contribution of S VIII emission line, we adopt the experimental line intensity ratio (0.75) between 61.645 and 52.781\AA , measured in EBIT facility by Lepson et al. (2005). The observed flux of the obvious emission around 52.780\AA is $0.39 \times 10^{-4} \text{phot.cm}^{-2}\text{s}^{-1}$. So S VIII occupies $\sim 39\%$ around 61.611\AA . By taking into account this blending, the observed intensity at 61.611\AA is 0.21 ± 0.07 relative to that of the line 55.346\AA as shown by the circle symbol in Fig. 4, which is slightly higher than the prediction over a large range of density. However, they agree within 2σ statistical errors. For the other two emissions at 61.702 and 61.846\AA , only the features of Si IX from $3s \rightarrow 2p$ transitions at 61.696 and 61.844\AA can be found in the present prediction and available database such as APEC and MEKAL. When the line intensities are normalized to that of 55.346\AA line, the observed ratios are significantly higher than the theoretical prediction (solid line) by an order of magnitude in typical coronal conditions, as shown by square and diamond symbols with 1σ error in Fig. 4.

A search in the Astrophysical Emission Code (APEC with version of 1.3.1) also indicates the emissivities of Si IX lines are the strongest. So the differences must be attributed to other explanations. The first thought is that whether the discrepancies are due to the contaminations from high-order spectral lines. In the spectrum of Procyon, no second- and third-order spectral lines of prominent lines in short wavelength range ($< 30\text{\AA}$) lie in this wavelength region. This encourages us to consider the incompleteness of model and/or the opacity effect. In the case of Fe XVII, Doron & Behar (2002) considered the effects of recombination, resonance excitation and ionization processes on the level

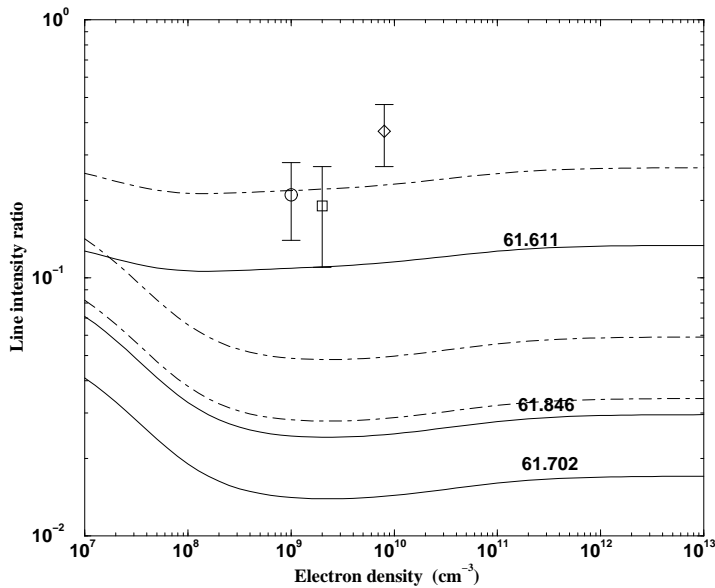


Fig. 4. Observed line ratios with 1σ error (symbols) of identified $3s \rightarrow 2p$ lines relative to that of the line at 55.346\AA . Theoretical predictions at the temperature $\log T_e(\text{K})=6.1$ are overlaid. The dot-dash lines represent agreement within a factor of 2.

populations, and made the theoretical prediction increase by 50%. The correct results shown a better agreement with observed ones for most stellar coronae. In the case of Si IX, observed ratio at 61.611\AA can agree with the prediction within 1σ uncertainty, if the indirect processes have a similar effect as in Fe XVII. For the other two possible $3s \rightarrow 2p$ emissions, the discrepancies being up to an order of magnitude, cannot be explained by the complete model. As suggested by Ness et al. (2003), the opacity effect is also not possible to be detected from the integrated spectrum for normal stars. So we suggest that the most possible reason might be the contamination of unknown emissions.

5 Conclusions

A detailed analysis of soft X-ray emissions of carbon-like silicon reveals that the ratio of Si IX lines around 55.246 and 55.346 Å is a good n_e -diagnostic method. By comparing the observed ratio with theoretical prediction, a lower limit of the density ($0.6 \times 10^8 \text{ cm}^{-3}$) was obtained for Procyon, which is the typical value of the solar quiescent corona. The constructed spectrum of Si IX suggests that the major contribution at 55.083 Å, and 61.611 Å should be assigned to Si IX.

In intensity ratios of $3s \rightarrow 2p$ transition lines of Si IX relative to that of $3d \rightarrow 2p$ line at 55.346 Å, significant discrepancies between observations and theoretical predictions are found in Procyon. For the $3s \rightarrow 2p$ line at 61.611 Å, the observation and theoretical prediction agree within a factor of 2, when the contamination arising from S VIII line (61.645 Å) has been considered. Here, an experimental ratio of 0.75 (Lepson et al. 2005) between S VIII lines at 61.645 and 52.781 Å was adopted to disentangle the blending. However, for other two possible $3s \rightarrow 2p$ lines of 61.792 and 61.848 Å, large differences (nearly an order of magnitude) cannot be explained by the uncertainty of atomic data and the resonant scatter effect. So we suggest that the most possible reason is contributions of unknown emissions, which may be addressed by further improvements in the soft X-ray spectral analysis.

Acknowledgments

This work is supported by the National Natural Science Foundation of China under Grant No. 10433010, 10403007 and 10521001.

References

- [1] Brinkman, A. C., Gunning, C. J. T., Kaastra, J. S., et al. 2000, *ApJ*, 530, L111
- [2] Canizares, C. R., Huenemoerder, D. P., Davis, D. S., et al. 2000, *ApJ*, 539, L41
- [3] Desai, P., Brickhouse, N. S., Drake, J. J., et al. 2005, *ApJ*, 625, L59
- [4] Doron, R., & Behar, E. 2002, *ApJ*, 574, 518
- [5] Gabriel, A. H., & Jordan, C. 1969, *MNRAS*, 145, 241
- [6] Gu, M. F. 2003, *ApJ*, 582, 1241
- [7] Güdel, M., Arzner, K., Audard, M., & Mewe, R. 2003, *A&A*, 403, 155
- [8] Güdel, M., Schmitt, J. H. M. M., Benz, A. O., & Elias, N. M. 1995, *A&A*, 301, 201
- [9] Lepson, J. K., Beiersdorfer, P., Behar, E., & Kahn, S. M. 2005, *ApJ*, 625, 1045
- [10] Liang, G. Y., Zhao, G., & Shi, J. R. 2006a, *AJ*, 132, 371
- [11] Liang, G. Y., Zhao, G., & Zeng, J. L. 2006b, *Atom. Data and Nucl. Data Tables* (accepted)
- [12] Matranga, M., Mathioudakis, M., Kay, H. R. M., & Keenan, F. P. 2005, *ApJ*, 621, L125
- [13] Mazzotta, P., Mazzitelli, G., Colafrancesco, S., & Vittorio, N. 1998, *A&AS*, 133, 403
- [14] Ness, J. -U., Güdel, M., Schmitt, J. H. M. M., Audard, M., & Telleschi, A. 2004, *A&A*, 427, 667
- [15] Ness, J. -U., Mewe, R., Schmitt, J. H. M. M. et al. 2001, *A&A*, 367, 282
- [16] Ness, J. -U., Schmitt, J. H. M. M., Audard, M., Güdel, M., & Mewe, R. 2003, *A&A*, 407, 347

- [17] Ness, J. -U., Schmitt, J. H. M. M., Burwitz, V., et al. 2002, *A&A*, 394, 911
- [18] Porquet, D., & Dubau, J. 2000, *A&AS*, 143, 495
- [19] Raassen, A. J. J., Mewe, R., Audard, M., et al. 2002, *A&A*, 389, 228
- [20] Ryans, R. S., Foster-Woods, V. J., Keenan, F. P., & Reid, R. H. G. 1999, *Atom. Data and Nucl. Data Tables*, 73, 1
- [21] Schmitt, J. H. M. M., Robrade, J., Ness, J. -U., et al. 2005, *A&A*, 432, L35
- [22] Siarkowski, M., Pres, P., Drake, S. A., White, N. E., & Singh, K. P. 1996, *ApJ*, 473, 470
- [23] Stelzer, B., & Schmitt, J. H. M. M. 2004, *A&A*, 418, 687
- [24] Testa, P., Drake, J. J., & Peres, G. 2004, *ApJ*, 617, 508